Gas-phase ozonolysis of trans-2-hexenal: Kinetics, products, mechanism and SOA formation

Asma Grira, Carmen Kalalian, J.N. Illmann, I. Patroescu-Klotz, G. El Dib, P. Coddeville, André Canosa, P. Wiesen, Estelle Roth, Abdelkhaleq Chakir, et al.

Gas-phase ozonolysis of trans-2-hexenal: Kinetics, products, mechanism and SOA formation

A. Grira[1,2], C. Kalalian[3], J.N. Illmann[4], I. Patroescu-Klotz[4], G. El Dib[2], P. Coddeville[1], A. Canosa[2], C. Coeur[5], P. Wiesen[4], E. Roth[3], A. Chakir[3], A. Tomas[1,*]

[1]*IMT Lille Douai, Institut Mines-Télécom, Univ. Lille, Centre for Energy and Environment, 59000 Lille, France*
[2]*Univ Rennes, CNRS, IPR (Institut de Physique de Rennes) -UMR 6251, F-35000 Rennes, France*
[3]*Groupe de Spectrométrie Moléculaire et Atmosphérique (GSMA), UMR CNRS 7331, Université de Reims, F-51687 Reims, France*
[4]*Institute for Atmospheric and Environmental Research, University of Wuppertal, Germany*
[5]*Laboratoire de Physico-Chimie de l'Atmosphère (LPCA) EA 4493, Université Littoral Côte d'Opale, 59140 Dunkerque, France*

* Corresponding author: alexandre.tomas@imt-lille-douai.fr

Submitted to Atmospheric Environment

Keywords: aldehyde; ozone; atmosphere; aerosol; kinetics

Credit author statement

AG, CK, JNI, IPK and AT did the experiments.

All authors contribute to the manuscript.

ABSTRACT

In this work, kinetics, product formation, chemical mechanism and SOA formation for the gas-phase reaction of trans-2-hexenal (T2H) with O_3 are examined using four complementary experimental setups at 298±2 K and atmospheric pressure. Product studies were conducted in two contrasted experimental conditions, with and without OH radical scavenger. The ozonolysis rate constant was determined in both static and dynamic reactors. An average reaction rate constant of $(1.52 \pm 0.19) \times 10^{-18}$ cm^3 $molecule^{-1}$ s^{-1} was determined. Glyoxal and butanal were identified as main products with molar yields of 59±15% and 36±9%, respectively, in the presence of an OH scavenger. Slightly lower values were obtained in the absence of scavenger. Acetaldehyde, propanal and 2-hydroxybutanal were also identified and quantified. A reaction mechanism was proposed based on the observed products. SOA formation was observed with aerosol mass yields > 13% for SOA masses of 400 µg m^{-3}. This work demonstrates for the first time that 2-alkenals ozonolysis can be a source of SOA in the atmosphere.

1. INTRODUCTION

It is now recognized that biogenic volatile organic compounds (BVOCs) play a major role in the chemistry of the troposphere from the local to the global scale[1]. Many BVOCs possess an unsaturated C=C double bond, which confers them a high reactivity towards the atmospheric oxidants[2]. Therefore, these biogenic species largely contribute to the formation of photochemical smog and tropospheric ozone on one hand and to the budget of hydroxyl radicals (OH) and the formation of secondary pollutants in the atmosphere on the other hand[2]. In addition, the oxidation of biogenic compounds yields less volatile species which could be a source of biogenic secondary organic aerosols (SOA)[3,4], one of the most uncertain factors in the global radiation budget[5].

While current research still focuses on the oxidation of the most abundant biogenic compounds in the atmosphere like isoprene and limonene[6,7], a number of unsaturated oxygenated compounds (aldehydes, ketones and alcohols) have been shown to be ubiquitously emitted by vegetation[1,8], especially when plants are damaged by biotic and/or abiotic stresses[9–11]. The emission of these species, so-called Green Leaf Volatiles (GLV), may have significant impacts on the environment and the air quality due to their high reactivity towards OH, O_3 and NO_3[9,12,13].

Trans-2-hexenal (T2H) is a GLV emitted from several different plants[14], green residues like oak and pine mulch[15] and leaf drying[16]. Once in the atmosphere, T2H can be removed by reaction with tropospheric oxidants such as OH[17–19] and NO_3 radicals[20], Cl atoms[21] and O_3 [20,22,23]. The reaction of T2H with O_3 proceeds as follows:

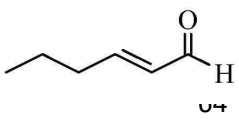

$$+ \quad O_3 \quad \xrightarrow{k_{03}} \quad \text{Products} \qquad \text{(R1)}$$

The rate constant was first determined by Atkinson et al.[20] at ambient temperature using the relative method. The significant error associated with their determination ($(2\pm1)\times10^{-18}$ cm^3 $molecule^{-1}$ s^{-1}) was assigned to a low consumption of T2H by O_3. An OH radical formation yield of ~0.62 was also estimated. However, the authors noted that there is a high degree of uncertainty in their determination. Grosjean et al.[23] conducted an extensive study and reported a rate constant ($(1.28\pm0.28)\times10^{-18}$ cm^3 $molecule^{-1}$ s^{-1} at 288 K) using an absolute method with T2H in excess over O_3. Both rate constants determined by Atkinson et al.[20] and Grosjean et al.[23] agree within the uncertainties. A range of carbonyl products was also observed in Grosjean's study[23] and their formation yields were calculated towards O_3 consumption. More recently, Kalalian et al.[22] investigated the kinetics of this reaction at 298

K using the absolute method with O_3 in excess over T2H. A consistent rate constant of $(1.37\pm0.03)\times10^{-18}$ cm^3 $molecule^{-1}$ s^{-1} was obtained. Apart from Grosjean et al.[23], no literature data are available on T2H + O_3 reaction products.

Regarding OH + T2H reaction, the three most recent kinetics studies[17–19] displayed consistent rate constant values, yielding an average OH rate constant of 4.24×10^{-11} cm^3 $molecule^{-1}$ s^{-1} at 298 K. NO_3 kinetics was investigated by Atkinson et al.[20] who determined a rate constant of 1.21×10^{-14} cm^3 $molecule^{-1}$ s^{-1} at 298 K. Thus, OH- and NO_3-initiated reactions represent the main removal of T2H in the atmosphere, with lifetimes of 6h and 8h, respectively, while O_3 reaction may only be competitive in polluted areas where high levels of ozone may be found[24]. Regarding the relevance of T2H atmospheric photolysis, Kalalian et al.[24] calculated an upper limit of 29 min assuming a quantum yield of 1, while O'Connor et al.[25] and Jiménez et al.[18] suggested that T2H photolysis constitutes a negligible pathway compared to its removal through tropospheric oxidants.

While these studies focused on the kinetics of these reactions, limited data exist concerning reaction products, with no data on the potential SOA formation in the troposphere. The main objective of the present study was to investigate thoroughly the reaction of T2H with ozone using several complementary experimental setups to improve our knowledge on T2H oxidation by O_3 in the atmosphere. The rate constant was measured with the absolute-rate method in both batch and flow reactors, aiming at enriching our knowledge on the kinetics of the studied reaction. Reaction products were identified with two techniques: Fourier Transform InfraRed (FTIR) spectroscopy and Gas Chromatography (GC) with mass spectrometry (MS). The capacity of T2H to form SOA by reaction with ozone was investigated for the first time using a Scanning Mobility Particle Sizer (SMPS) device and aerosol yields were evaluated.

2. MATERIALS AND METHODS

2.1. Reactors, conditions and reagents

Four experimental setups were used in the present study: A Laminar Flow Reactor (LFR)[7,26] and an Atmospheric Simulation Chamber (ASC)[27,28] at IMT Lille Douai, a glass chamber[29] at Wuppertal University and a Rigid Atmospheric Simulation Chamber (RASC)[22,30] at GSMA/Reims University. While these reactors are briefly described in this section, the reader is invited to refer to the cited literature for more details. A summary of the experimental

conditions and analytical techniques is provided in Table 1. The compounds used with stated purities are reported in SI.

2.1.1 LFR/IMT Lille Douai (France)

The LFR was used to study the kinetics of T2H + O_3 in a dynamic flow reactor in the absence of an OH scavenger. The reactor consists in a vertical Pyrex tube of 1 m length and 10 cm inner diameter working with a total flow of 2.3 L min^{-1}. Accurate concentrations of T2H were prepared in canisters through vaporization of small aldehyde aliquots and filled with air to a pressure of approximately 3 bars. A small flow (typically 10 mL min^{-1}) from the canister was diluted by purified air and then sent to the reactor injection head. GC coupled to a thermal desorption system was used in online mode for the sampling and analysis of the organic reactant. A double detection by flame ionization (FID) and mass spectrometry (MS) was operated on the GC. The initial concentration of T2H was calculated from the FID signal using the calibration curve determined in preliminary work. Ozone was produced by flowing oxygen through an ozone generator (TEI 146) and was analyzed by a UV-absorption based analyzer.

2.1.2 ASC/IMT Lille Douai (France)

The ASC was used to determine the rate constant with and without OH scavenger (cyclohexane) and to investigate the SOA formation from the studied reaction. It consists of a Teflon bag of about 300 L inside a wooden box, which ensures darkness during experiments. Two ports installed on the reactor walls allow filling and emptying of the reactor and taking gas samples for analyses. Ozone was produced by flowing purified air through a high-voltage discharge generator (C-Lasky Ozone Generator). Ozone was measured using the same analyzer as in LFR experiments. T2H and cyclohexane were quantified by FTIR using a 2 L White cell with 10 m optical path. Mid-IR spectra were recorded every 4 min with a resolution of 0.5 cm^{-1} (100 spectra co-added). The initial concentration of T2H was calculated from IR spectra using a calibration curve determined in preliminary work. The characterization of particles in the reactor was carried out with an SMPS with a sampling flow of 0.6 L min^{-1} at a scan rate of 2.5 min (particle size distribution 10 – 408 nm).

2.1.3 480-L glass-Wuppertal University (Germany)

The 480-L glass chamber, characterized with a 3 m length and an inner diameter of 45 cm, was used to study the reaction products without adding an OH scavenger. Yet, some

experiments were performed with dimethyl-ether as OH tracer. Different ports allow the addition of both reagents and bath gases. Ozone was generated by a homemade device via corona discharge in a flow of oxygen. To evacuate the chamber, a pumping system made of a roots pump backed by a double stage rotary pump is used. In order to ensure the homogeneity of the reaction mixture, a Teflon fan is mounted inside the reactor. The concentrations of reactants and products were determined by IR spectroscopy using a FTIR spectrometer with a multi-reflection mirror system operating at an optical path length of 50.4 m, mounted internally in the chamber. Spectra were recorded every 5 min with a spectral resolution of 1 cm^{-1} (70 spectra co-added). The initial concentration of T2H was obtained using a calibration method described previously[31].

2.1.4 RASC - GSMA Reims (France)

The RASC was used to determine the reaction products in the presence of an OH radical scavenger. It is a 63-L triple jacket Pyrex cell with an inner diameter of 20 cm and a total length of 2 m. A set of spherical golden mirrors placed in the cell ensures multiple reflections and allows us to get an optical path of 56 m. This chamber was coupled to an FTIR spectrometer and to a GC/MS. Spectra were recorded every 3 min with a spectral resolution of 2 cm^{-1} (100 spectra co-added). Ozone was produced according to the procedure given by Griggs[32]. Its concentration was monitored by UV absorption spectroscopy using a CCD camera and then continuously driven into the simulation chamber. The concentrations of the reagents and the products formed during the ozonolysis reaction were monitored by IR and by Solid Phase Micro-Extraction (SPME)-GC/MS (see SI section B for more details) and were corrected for the pressure increase (about 200 Torr per hour).

2.2. Kinetic measurements

All experiments in ASC and LFR were carried out under pseudo-first-order conditions where the initial aldehyde concentration was in excess by a factor of 10 or more compared to that of ozone (Table 1). With OH radicals being produced in the O_3 + T2H reaction[20] and OH reacting fast with T2H ($k(OH+T2H) = 4.24\times10^{-11}$ cm^3 $molecule^{-1}$ s^{-1} [17–19]), some experiments in the chamber were performed with cyclohexane as OH scavenger.

In the ASC reactor, a typical experiment was performed as follows: T2H was introduced into the reactor and allowed to homogenize for around 30 min. Four samples were then taken to determine its initial concentration. Where applicable, a sufficient quantity of cyclohexane was added to trap about 94% of the formed hydroxyl radical (see SI section C) and the

T2H/cyclohexane mixture was allowed to homogenize for 1 hour. Subsequently, three samples were taken to quantify the initial concentration of both T2H and cyclohexane and to verify that there is no interference between the selected IR bands of the two compounds. Ozone was then introduced into the reactor and continuous O_3 measurements were performed over time.

Concerning experiments carried out in the LFR, ozone was introduced in a continuous flow through the injection head which was moved up and down to change the reaction time from 30 s to about 3 min. The remaining ozone is measured for each position of the reactor's head.

Ozone wall losses ($k_{wall\ loss}$) in the ASC chamber and the LFR reactor were estimated in preliminary tests. The obtained $k_{wall\ loss}$ were of 3×10^{-5} s^{-1} and 1.55×10^{-6} s^{-1} in the ASC and LFR, respectively. T2H wall losses were also investigated both in the ASC and the LFR and were found to be negligible.

The consumption of ozone can be expressed as follows:

$$-\frac{d[O_3]}{dt} = k[T2H]_0[O_3] + k_{wall\ loss}[O_3] = k'[O_3] \quad \text{(Eq. 1)}$$

where $k' = k[T2H]_0 + k_{wall\ loss}$. Since the aldehyde is in excess over O_3, the integration of Eq. 1 gives:

$$ln\left(\frac{[O_3]_0}{[O_3]}\right) = k't \quad \text{(Eq. 2)}$$

where $[T2H]_0$ and $[O_3]_0$ are respectively the initial concentrations of T2H and ozone and $[O_3]$ is the concentration of ozone at time t. Eq. 1 shows that the measured ozone decays are only dependent on T2H concentration and O_3 wall losses and will thus not be affected by the presence or absence of an OH scavenger[23]. In the case of LFR, the reaction time is calculated using the expression computed by Duncianu et al.[26] taking into account the slight parabolic form of the flow rate profile in the reactor[26]. According to Eq. 2, the slope of the linear fitting of $ln\left(\frac{[O_3]_0}{[O_3]}\right)$ versus time gives the pseudo-first-order rate constant k'. The ozonolysis rate constant k can be determined from the slope of the plot of k' as a function of $[T2H]_0$.

2.3. Product analysis

The experiments were performed in the 480-L glass reactor without OH scavenger and in the RASC chamber using cyclohexane as OH scavenger (see Table 1 for initial concentrations).

Product yields Y_{Prod} were obtained from the plot of the product mixing ratios [Prod] vs. aldehyde consumption, Δ[T2H], according to Eq. 3.

$$Y_{Prod}\ (\%) = \frac{[Prod]}{\Delta[T2H]} \times 100 \qquad \text{(Eq. 3)}$$

2.3.1. Product analysis in the 480-L glass reactor

The products were identified and quantified by FTIR spectroscopy, where recorded spectra were compared with references available in IR databases at the Wuppertal laboratory. The quantification of butanal was done using tabulated IR absorption cross sections determined in the same system. Glyoxal was quantified using absorption cross sections determined by Volkamer et al.[33]. T2H, butanal and glyoxal concentrations were retrieved using the following IR absorption bands centered at 1150 and 2726 cm^{-1}, 1126 and 2712 cm^{-1}, and 2835 cm^{-1}, respectively, by iterative subtraction of calibrated reference spectra. Uncertainties on Y_{Prod} were obtained by adding errors on Δ[T2H] (estimated at 14%) and errors on [Prod] arising from uncertainties on both absorption cross sections (5%) and subtraction procedure (10%). Overall uncertainties on Y_{Prod} calculated by error propagation were of the order of 20%.

2.3.2. Product analysis in the RASC chamber

Two techniques were used to identify and quantify the products in the RASC chamber: FTIR spectroscopy and SPME-GC/MS. The derivatization conditions were taken from Reisen et al.[34] and are summarized in SI (section B). During each experiment, T2H and cyclohexane were driven by an air flow into the simulation chamber. The ozonolysis reaction started following the addition of ozone into the chamber through a continuous flow. The sampling was carried out every 15 min and the analyses were performed by GC-MS. At the same time, IR spectra were recorded every 3 min and T2H (1615-1674 cm^{-1}) and 2-hydroxybutanal (1043-1077 cm^{-1}) bands were processed and integrated. The areas of the chromatographic peaks or IR bands were related to the concentration of the product through calibration curves previously prepared for the different compounds.

The formation yields of all stable primary and secondary products were determined by SPME-GC/MS. IR spectra were only used to identify and quantify 2-hydroxy-butanal (IR reference spectrum in Figure S1). The obtained yields correspond to the average of three experiments. Overall uncertainties on the yields were calculated by error propagation considering both the

repeatability of the measurements and errors on spectra subtractions, peak integrations and calibration procedures. The overall uncertainties on yields vary from 25-30%.

2.4. SOA formation

Particle formation was studied in ASC in the absence of OH scavenger. Preliminary tests were performed to ensure that no particle formation occurs when either T2H or ozone was introduced alone in the chamber. Continuous SMPS measurements started just after ozone injection until a steady state of particle mass formation was reached.

The relatively high surface-to-volume (S/V) ratio of the reactor (~ 7 m^{-1}) inevitably led to semi-volatile gas and particle losses on the walls[35]. Aerosol wall losses were determined for each experiment after maximum aerosol formation, resulting in first-order decay rates of 10-20% h^{-1}. The aerosol mass concentrations measured in the present work were then corrected for wall losses. SOA formation yields (Y_{SOA}) were calculated according to the following expression:

$$Y_{SOA}\ (\%) = \frac{M_0}{\Delta[T2H]_f} \times 100 \qquad \text{(Eq. 4)}$$

where M_0 is the corrected maximum mass concentration of particles formed and $\Delta[T2H]_f$ is the consumed mass concentration of T2H at the same time. Total aerosol mass concentrations M_0 were calculated from the measured number size distributions assuming spherical particles with a density of 1 g cm^{-3}. The experimental conditions including, initial concentrations and analytical techniques are summarized in Table 1.

3. RESULTS AND DISCUSSION

3.1. Kinetics

The pseudo-first order rate constant k' was determined according to Eq. 2 from the plot of $\ln([O_3]_0/[O_3])$ versus reaction time (Figures S2 (chamber) and S3 (flow reactor)). The data were fitted with linear regression lines. Plots in Figure S2 and S3 display a good linearity with high correlation coefficients ($R^2 > 0.90$). A linear regression of the k' data vs. $[T2H]_0$ (Figure 1) yields the second order rate constant. A value of $k(T2H + O_3) = (1.52 \pm 0.19) \times 10^{-18}$ cm^3 $molecule^{-1}$ s^{-1} was obtained where the statistical uncertainty represents 2σ (fitting error). This k-value comes from a fit on both ASC and LFR data.

Statistical errors on k' (2σ) resulting from the fitting procedure and reported on Figure 1 are 2-6% for ASC data and 9-26% for LFR data. $[T2H]_0$ is determined with an uncertainty of about 10% arising from the calibration procedure. Systematic errors on $[T2H]_0$ that may impact k values are probably negligible because of the high volatility of T2H leading to a quantitative injection in the reactor. Propagating the errors results in a global uncertainty on k of about 16%.

The obtained value is in good agreement with data obtained in simulation chambers (Table 2). The rate constant was first determined by Atkinson et al.[20] using the relative kinetic method. They reported a value of 2×10^{-18} cm^3 $molecule^{-1}$ s^{-1} with an uncertainty of 50%. Grosjean et al.[23] used pseudo-first order conditions with T2H in excess and obtained a value of $(1.28\pm0.28)\times10^{-18}$ cm^3 $molecule^{-1}$ s^{-1}. More recently, Kalalian et al.[22] obtained $(1.37\pm0.03)\times10^{-18}$ cm^3 $molecule^{-1}$ s^{-1} in absolute rate experiments. As can be seen, the present value of $(1.52\pm0.19)\times10^{-18}$ cm^3 $molecule^{-1}$ s^{-1} agrees very well with those of Grosjean et al. and Kalalian et al. and is consistent with that of Atkinson et al. taking into account the uncertainties. The present work represents the first determination of k(T2H + O_3) in a flow reactor. The present results also complement the study of Grosjean et al.[23] which was carried out using the absolute kinetics method and T2H in excess, yet with a much narrower range of T2H concentrations than our study (Table 2). The very good agreement with Grosjean et al. adds to the reliability of the results.

The T2H + O_3 reaction rate constant is significantly higher than that reported for acrolein (a mono-substituted unsaturated compound, 3.5×10^{-19} cm^3 $molecule^{-1}$ s^{-1})[36] whereas it is in the same order of magnitude as that of other longer (bi-substituted) unsaturated aldehydes: crotonaldehyde ($(1.58\text{-}1.74)\times10^{-18}$ cm^3 $molecule^{-1}$ s^{-1})[37,38]; 2-pentenal (1.6×10^{-18} cm^3 $molecule^{-1}$ s^{-1})[38], and a series of linear C_7-C_9 unsaturated aldehydes: 2-heptenal, 2-octenal and 2-nonenal ($(2.05\text{-}2.47)\times10^{-18}$ cm^3 $molecule^{-1}$ s^{-1})[39]. This suggests the role of the C=C double bond substitution on the reactivity of alkenals towards O_3, with a positive inductive effect on the electronic density of the C=C bond and an increase of the O_3 addition rate constant from mono- to bi-substituted alkenals.

McGillen et al. proposed a structure-activity relationship for the ozonolysis kinetics of a number of unsaturated compounds including aldehydes[40]. They underlined the role of the inductive effect on the reactivity of these species. For T2H, an ozone rate constant of 2.0×10^{-18} cm^3 $molecule^{-1}$ s^{-1} can be calculated, which is in good agreement with experimental

findings. Comparing the rate constant for the ozonolysis of T2H to that of trans-2-hexene (155×10^{-18} cm^3 $molecule^{-1}$ s^{-1})[41] shows a 100 times higher rate constant for the homologous alkene compared to the studied aldehyde. A similar trend is observed for crotonaldehyde/trans-2-butene[41,42] and 2-pentenal/trans-2-pentene[41]. This shows the strong deactivating effect of the carbonyl group on the reactivity of the C=C double bond towards ozone through the conjugation of the two π systems (C=O and C=C).

3.2. Product formation

3.2.1. Product formation investigated in 480-L glass reactor

Seven experiments were performed in the 480-L glass reactor, out of which three included dimethyl ether (DME) used as OH radical tracer. Based on the DME pseudo-first order consumption, an upper limit of 10^6 molecules cm^{-3} was estimated for the concentration of OH radicals in this reaction system. Butanal and glyoxal were identified as the major primary products by FTIR. The fine spectral features of glyoxal can be clearly observed in the 2800-2850 cm^{-1} region while the presence of butanal is evidenced near 2700 cm^{-1} (Figure 2). After subtracting T2H and O_3 as well as glyoxal and butanal, the residual spectra show features that indicate the presence of products containing carbonyl and possibly OH moieties.

Concentration-time profiles of T2H, butanal and glyoxal are presented in Figure S4 together with the carbon balance calculated as molar yield. Yield plots of the concentrations of the primary products as a function of consumed T2H are shown in Figure 3, for all performed experiments. For butanal and glyoxal, molar yields of 33±7% and 48±10%, respectively, were obtained, where the errors (2σ) represent estimated total uncertainties of ~20% (see section 2.3.1). These yields were not corrected for potential OH losses. The OH concentration evaluated upon tracer data (10^6 molecules cm^{-3}) is rather small to compete significantly with the T2H + O_3 reaction considering the ozone concentrations used, namely $(4\text{-}8)\times10^{14}$ molecules cm^{-3}.

The formation of propanal could be observed in all experiments (see Figure S5) but due to overlapping of absorption features it cannot be quantified accurately. An upper limit of 8% (molar yield) can be estimated using the absorption band centered at 2992 cm^{-1}. Similarly, it is not possible to quantify acetaldehyde in the residual spectra although there are features indicating its formation (Figure S5). From the residual spectra and using the absorptions

centered at 1352 and 2706 cm^{-1}, respectively, an upper limit of 10% can be calculated for the molar yield of acetaldehyde.

Although a significant increase was observed for the intensity of the specific absorptions attributed to CO and CO_2, their quantification is not possible under the present experimental setup due to interferences of these compounds present in the dry air used to flush the transfer optics housing between the chamber and FTIR spectrometer. Formaldehyde was not observed in the IR spectra. Considering the detection limit of 200 ppb in our system, an upper limit of 4% can be deduced for the molar yield of formaldehyde, if any.

3.2.2. Product formation investigated in RASC chamber

Five carbonyl compounds: glyoxal, butanal, propanal, acetaldehyde and 2-hydroxybutanal were positively identified in the gas-phase reaction of T2H with O_3, in the presence of cyclohexane as OH scavenger. CO was not observed while CO_2 analysis was precluded due to the lack of a specific instrument. 2-Hydroxybutanal was detected both in the residual IR spectra (after subtraction of the known features, a significant absorption band persisted between 1043 and 1077 cm^{-1} which can be assigned to 2-hydroxybutanal) and by GC/MS through the corresponding oxime. The temporal evolution of the molar fractions of T2H and of the products formed during the ozonolysis reaction as well as the carbon balance are presented in Figure S6. Product concentrations are relatively stable after 60 min. The carbon balance decreases with the T2H + O_3 reaction progress, indicating the formation of other undetected products. Formation yields of primary and secondary products were determined by plotting product concentrations as a function of the consumed T2H (Figure 4). The 2-hydroxybutanal yields obtained by IR and GC/MS techniques were in good agreement with a difference lower than 20%. The products identified and quantified by FTIR (480-L chamber, RASC) and GC/MS (RASC) are summarized in Table 3.

3.2.3. Comparison with literature data

Glyoxal and butanal have been identified as main products in both the 480-L reactor and RASC. The product yields obtained in both set-ups are in good agreement (48±10% and 33±7% in the 480-L reactor, Figure 3, 59±15% and 36±9% in RASC, Figure 4) within the uncertainties and thus seem not to be influenced by the formation of OH during the ozonolysis reaction.

In the 480-L chamber, the concentration of OH radicals was estimated based on the tracer (DME) consumption to vary from 10^5 to 10^6 molecules cm^{-3}. By using the method described

by Klotz et al.[43] to correct for the OH reaction, this accounts for up to 10% of the overall consumption of trans-2-hexenal. Further, this finding suggests a much lower OH yield from the T2H + O_3 reaction as previously reported[20]. A former study[44] on the ozonolysis of trans-2-alkenals estimates an OH production of up to 15% which is supported by our results using DME (Figure S7). This indicates that the errors in the experimentally determined yields for butanal and glyoxal are higher than the effect of the presence of OH in the reaction system. Nevertheless, the yields are slightly below the values obtained when using an OH scavenger (RASC).

The results are summarized in Table 3 together with literature data[23]. The glyoxal yields determined here are in good agreement with the previous study carried out by Grosjean et al., who normalized the carbonyl concentration to the concentration of reacted ozone. In both chambers in this study, the butanal yield is somewhat lower than previously reported. Unlike Grosjean et al., whose results suggest that both main products are formed in equal portions, the present study indicates a slight preference for the pathway yielding the bicarbonyl compound, namely glyoxal. The ozonolysis of asymmetric alkyl-substituted alkenes is known to favor the formation of the most substituted bi-radical due to hyperconjugation[23,45]. Further, studies carried out on the ozonolysis of oxygenated alkenes indicate that the decomposition of the primary ozonide displays a preference for the pathway yielding an oxygenated carbonyl[46–48]. Hence, the formation of the alkyl-substituted bi-radical and the formation of glyoxal could be favored. However, the limited number of reported data for the ozonolysis of trans-2-alkenals (C_3-C_9, Table S1) does not indicate a clear trend to support this observation.

When comparing with the studies performed by Grosjean and co-workers, one notes that they worked at a relative humidity of 55%[23] whereas the present study was done under dry conditions (RH $\leq$ 1%). At least for glyoxal, it was determined that aerosols represent a significant sink due to reactive uptake on surface,[4,49,50] especially at high RH[51,52]. For butanal and trans-2-hexenal, presently no such information is available, therefore further considerations would be highly speculative. The fate of the stabilized Criegee Intermediates (CI) that are expected to come from O_3 + T2H is also highly dependent on the amount of water available.[3,7] Since butanal and glyoxal do not come from CI, their yields are not expected to be impacted by RH.

Acetaldehyde, propanal and 2-hydroxybutanal were undoubtedly quantified only in RASC. The yield of acetaldehyde is in excellent agreement with the previous determination by

Grosjean et al.[23]. There is evidence of formation of propanal and acetaldehyde in the 480-L chamber (Figure S5), however the quantification limit of the system and the superposition of the spectra allows only the estimation of upper limits for their yields. The presence of butanoic acid in the spectra obtained from the 480-L chamber cannot be ruled out as its spectral features can be "hidden" beneath the residual unidentified absorptions (Figure S8).

The residual spectra of the experiments with OH scavenger (Figure 2, panel E), after subtracting T2H, ozone and the main products, contain additional absorption features which suggest formation of unidentified carbonyl containing compounds and which differ from the absorption of 2-hydroxybutanal recorded in RASC. However, the characteristic absorption system between 3000 cm^{-1} and 2700 cm^{-1} looks similar to the residual spectra reported by Colman et al.[44]. They studied the ozonolysis of longer trans-2-alkenals and tentatively assigned their residuals to the corresponding 2-oxoaldehydes. Grosjean et al.[23] identified 2-oxobutanal in the ozonolysis of trans-2-hexenal with a yield of 7.4±0.6%. However, they argued that, due to the use of dinitrophenylhydrazine derivatization, followed by offline high performance liquid chromatography to identify and quantity products, they were not able to distinguish between the 2-oxo and the 2-hydroxyaldehyde. The results obtained presently in RASC indicate that rather 2-hydroxybutanal is formed than 2-oxobutanal.

The organic gas-phase carbon balance calculated in RASC is lower than 100% (down to 60% at the end), and even lower in the 480-L chamber. One reason is the impossibility to determine all products formed in such a complex system, as stated above. The ozonolysis reactions are generally known to deliver poor overall yields as the identification and quantification of all products often fails[53]. On the other hand, the formation of aerosol particles observed here strongly suggests that the adsorption on particles and/or heterogeneous chemistry is possibly responsible for incomplete carbon numbers. At this time, without knowledge on the particle composition, it is not possible to make a quantitative estimation of the contribution of aerosols to the carbon balance in the ozonolysis of trans-2-hexenal.

3.2.4. Mechanism

The products identified within this study support a classical approach, namely the electrophilic addition of O_3 to the double bond followed by the decomposition of the ozonide into a primary carbonyl and a Criegee biradical (CI)[3]. A reaction mechanism for T2H ozonolysis is proposed in Figure 5 based on the product analysis from the RASC and 480-L chambers.

The first step in the ozonolysis of trans-2-hexenal will produce an asymmetrical ozonide. As displayed in Scheme 1, there are two possibilities for it to dissociate.

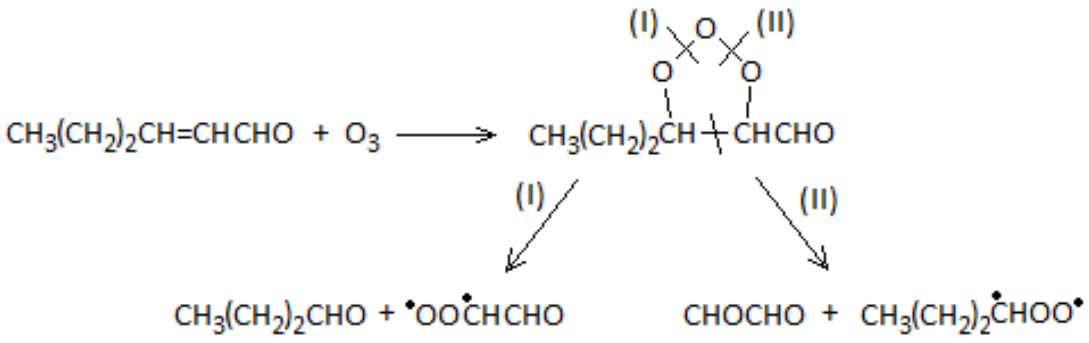

Scheme 1. Ozone addition to T2H followed by decomposition of the ozonide according to two channels: (I) forming butanal and (II) forming glyoxal as primary carbonyls.

Channel (I) leads to the formation of butanal identified and quantified in this work as a major product. The •OO•CHCHO biradical resulting from channel (I) could evolve into two pathways (Figure 5):

a. Formation of formaldehyde and CO_2: Formaldehyde was not observed in the FTIR spectra, neither in the 480-L nor in the RASC chamber. Although an increase in the intensity of the characteristic CO_2 absorptions bands (2289-2388 cm^{-1}) was observed, its quantification was not possible under the given experimental conditions. According to the limit of detection for formaldehyde in the 480-L chamber, the branching ratio for this channel, if occurring, is below 0.04.

b. OH and CHOCO• formation. The CHOCO• radical could evolve into CO_2 and CHO•, the latter reacting with O_2 to form HO_2 and CO. The formation of OH radicals was observed in the 480-L chamber in absence of scavenger, using DME as a tracer. Carbon monoxide formation was unambiguously observed in the IR spectra recorded in the 480-L chamber but no quantification was possible for reasons mentioned earlier. We envision a systematic determination of both CO and OH yields as the object of a future study.

Channel (II) leads to the formation of glyoxal, another major product identified and quantified in our study. The vibrationally excited CI from channel (II) could either be stabilized by

collision or undergo fast unimolecular decomposition i) via 1,5-H shift and hydroperoxide formation (Scheme 2) or ii) to form OH and an alkoxy radical that leads to propanal (Figure 5).

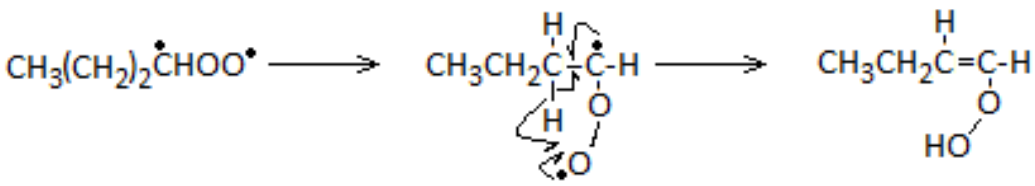

Scheme 2. The hydroperoxide channel – the fate of the excited CI resulting from channel (II).

The hot hydroperoxide resulting from channel (II) as presented in Scheme 2 can evolve into four different pathways (Figure 5)[54]:

a'. Rearrangement into and stabilization of a β-hydroxycarbonyl: 2-hydroxybutanal was observed in RASC with a formation yield of 18±6%;

b'. Formation of H_2 and 2-oxobutanal: the formation of 2-oxobutanal in the present study cannot be ruled out;

c'. Decomposition into CHO• + α-hydroxyalkyl, the latter yielding propanal, observed in the present work in the experiments with an OH scavenger and quantified with a formation yield of 19±5% in RASC; CHO• will yield HO_2 + CO; as mentioned above, CO formation was observed by IR but not quantified;

d'. Release of an OH radical and formation of CH_3CH_2•CHCHO. In the presence of O_2, this radical will form the oxy radical CH_3CH_2CHO•CHO. The oxy radical further chemistry may evolve toward production of acetaldehyde, glyoxal, propanal and 2-oxobutanal. Acetaldehyde was identified and quantified in our study with a formation yield of around 10%.

In the proposed mechanistic scheme, propanal, acetaldehyde and 2-hydroxybutanal are solely formed from CI (II) through the hydroperoxide channel (pathways a', c' and d'). The yield for glyoxal formed via route d'_1 should to be equal to the acetaldehyde yield (see Figure 5). It is worth noting that for RASC (taking into account the uncertainties) the sum of propanal, acetaldehyde and 2-hydroxybutanal yields (47%) differs by roughly 10% from the glyoxal yield (59%). This is consistent with the proposed mechanism.

In addition to the evolution routes mentioned above, the stabilized biradical $CH_3(CH_2)_2C^{\bullet}HOO^{\bullet}$ can isomerize into a dioxy biradical and form butanoic acid (Scheme 3)[3,55].

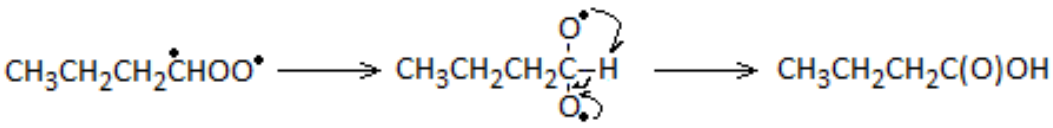

Scheme 3. Formation of butanoic acid from the stabilized CI $CH_3(CH_2)_2C^{\bullet}HOO^{\bullet}$ arising from channel (II).

No certain identification of butanoic acid is possible due to IR absorption band overlapping in the residual spectra (see Figure S8). Thus, the formation of an organic acid cannot be excluded.

3.3. SOA formation

Aerosol formation was investigated in the 300-L Teflon chamber. SOA growth is presented below in terms of total produced mass concentrations and aerosol yields.

3.3.1 Particle mass concentrations

Figure 6 shows particle formation, in terms of corrected mass concentration M_0, as a function of time in the ASC chamber. According to Figure 6, particle formation in ASC is very fast and occurred as soon as ozone is injected. SOA mass concentrations reach a plateau after roughly 50 min reaction time after which M_0 stabilizes. It is important to stress that the decreasing carbon balance observed with reaction time could be partly explained by the increasing organic matter in the condensed phase.

3.3.2 Yield plots

From SOA mass concentrations at the maximum of the plateau together with the corresponding T2H consumption, aerosol yields can be determined according to Eq. 4. Figure 7 displays the aerosol yield as a function of aerosol mass concentration for the experiments carried out in ASC. The oxidation of 1.6 to 10.2 ppm of aldehyde by increasing amount of ozone led to SOA yields of 3.2% to 13.4% for T2H corresponding to SOA mass

concentrations up to 418 µg m^{-3}. The Y_{SOA} vs. M_0 data were fitted using the one-product model from Odum et al.[56] that translates into the following equation:

$$Y_{SOA} = M_0 \left(\frac{\alpha K_{om}}{1 + M_0 K_{om}} \right) \quad \text{(Eq. 5)}$$

where α is the mass-based gas-phase stoichiometric coefficient of a model product and K_{om} represents its gas-particle partitioning equilibrium constant. α represents the total amount of semi-volatile products present in the gas- and aerosol- phases. A least-square regression on the data yields gives the following parameters: α = 0.22±0.08 and K_{om} = (3.2±2.4)×10^{-3} m^3 µg^{-1}. Uncertainties represent two standard deviations (2σ). Comparing α with Y where Y corresponds to the semi-volatile products in the particle phase indicates that only a fraction of the semi-volatile products go into the condensed phase.

3.3.3 Atmospheric impact

The present study shows for the first time that ozonolysis reactions for T2H can be a significant source of particles. As shown in Figure 7, an increase in the aerosol mass concentration leads to higher yields, consistent with increased surface area onto which condensation/partitioning of condensable reaction products can occur. In indoor environments where particle concentrations are often much higher than outdoor, sometimes by one order of magnitude[57–59], up to 10% of the reacted T2H can go into the particulate phase, provided sufficient O_3 are present indoors. Further investigations in larger reactors are clearly needed to thoroughly quantify the potential of T2H and other alkenals to form SOA through ozonolysis. In the atmosphere where the atmospheric fate of T2H is mainly governed by its reaction with OH and NO_3,[24] the impact of SOA formation from T2H ozonolysis is limited. The situation may be reversed indoors where OH and NO_3 radical concentrations are generally much lower than outdoors.[60] Under these conditions, indoor sources of ozone – outdoor air as well as photocopiers and air purifiers – could make O_3 a significant oxidant indoors,[60] thus potentially enhancing the contribution of T2H to SOA indoors. In some specific indoor cases, however, like high HONO levels or high-O_3 and low-NO concentrations, OH and NO_3 can reach high concentrations making T2H oxidation by OH and/or NO_3 significant indoors.[60]

4. CONCLUSION

In this work, the kinetics of the reaction of T2H with ozone has been investigated for the first time using a flow reactor and the absolute method. Additional experiments using a static

atmospheric simulation chamber were performed. Both experimental set ups yield consistent results and show very good agreement with the literature data.

The mechanistic studies carried out in the present work showed that the ozonolysis of T2H leads to the formation of carbonyl compounds as primary products, namely glyoxal and butanal, as well as acetaldehyde, propanal and 2-hydroxybutanal. In the presence of an OH scavenger, molar yields of 59±15% and 36±9% were obtained for glyoxal and butanal, respectively, in satisfactory agreement with the only reported study up to date[23]. In the absence of an OH scavenger, the yields of glyoxal and butanal did not differ significantly, within the error limits, which suggests that secondary OH processes are of minor importance. A detailed chemical reaction mechanism is proposed upon the identified reaction products. The total yields of primary carbonyl products range between 81% and 95%. A slight preference is directed towards the formation of the bi-radical not containing the aldehyde function. These results on the C_6 alkenal complete the missing puzzle data of previous studies of C_3-C_9 trans-2-alkenals.

Finally, the present study constitutes the first investigation of aerosol formation from the ozonolysis of a trans-2-alkenal species, to the best of our knowledge. T2H ozonolysis is shown to only slightly contribute to particle loadings in the atmosphere. Further work is clearly needed to improve our understanding of SOA contribution from oxygenated unsaturated compounds, which are ubiquitous species emitted by vegetation. Very recently, Liu et al.[61] suggested that alkenals contributed up to 34% of the SOA observed from the photo-oxidation of vegetable oil emissions. Experimental work on reaction products and SOA formation from T2H + OH is under progress, aiming at unravelling the role of this reaction in the atmospheric chemistry of T2H.

Acknowledgments

IMT Lille Douai acknowledges funding by the French ANR agency under contract No. ANR-11-LabX-0005-01 CaPPA (Chemical and Physical Properties of the Atmosphere), the Région Hauts-de-France, the Ministère de l'Enseignement Supérieur et de la Recherche (CPER Climibio) and the European Fund for Regional Economic Development. Part of this work has received funding from the European Union's Horizon 2020 research and innovation program through the EUROCHAMP-2020 Infrastructure Activity under grant agreement No 730997. A. Grira is grateful for a PhD grant from Brittany Region and IMT Lille Douai. Authors from French laboratories acknowledge the INSU-LEFE-CHAT program for funding this research.

Bibliography

[1] A. Guenther, C. N. Hewitt, D. Erickson, R. Fall, C. Geron, T. Graedel, P. Harley, L. Klinger, M. Lerdau, W. A. Mckay, T. Pierce, B. Scholes, R. Steinbrecher, R. Tallamraju, J. Taylor, P. Zimmerman, *J. Geophys. Res. Atmospheres* **1995**, *100*, 8873–8892.

[2] R. Atkinson, J. Arey, *Atmos. Environ.* **2003**, *37*, S197–S219.

[3] D. Johnson, G. Marston, *Chem. Soc. Rev.* **2008**, *37*, 699–716.

[4] M. Hallquist, J. Wenger, U. Baltensperger, Y. Rudich, D. Simpson, M. Claeys, J. Dommen, N. M. Donahue, C. George, A. H. Goldstein, J. F. Hamilton, H. Herrmann, T. Hoffmann, Y. Iinuma, M. Jang, M. E. Jenkin, J. L. Jimenez, A. Kiendler-Scharr, W. Maenhaut, G. McFiggans, T. F. Mentel, A. Monod, A. S. H. Prévot, J. H. Seinfeld, J. D. Surratt, R. Szmigielski, J. Wildt, *Atmospheric Chem. Phys.* **2009**, *9*, 5155–5236.

[5] T. F. Stocker, D. Qin, G. K. Plattner, M. Tignor, S. K. Allen, J. Boschung, A. Nauels, Y. Xia, V. Bex, P. M. Midgley, *IPCC, 2013: Climate Change 2013: The Physical Science Basis.*, Cambridge University Press, **2013**.

[6] J. A. Thornton, J. E. Shilling, M. Shrivastava, E. L. D'Ambro, M. A. Zawadowicz, J. Liu, *ACS Earth Space Chem.* **2020**, *4*, 1161–1181.

[7] W. Ahmad, C. Coeur, A. Cuisset, P. Coddeville, A. Tomas, *J. Aerosol Sci.* **2017**, *110*, 70–83.

[8] J. Laothawornkitkul, J. Taylor, N. D. Paul, C. N. Hewitt, *New Phytol.* **2009**, *183*, 27–51.

[9] J. Penuelas, M. Staudt, *Trends Plant Sci.* **2010**, *15*, 133–144.

[10] M. Toome, P. Randjärv, L. Copolovici, Ü. Niinemets, K. Heinsoo, A. Luik, S. M. Noe, *Planta* **2010**, *232*, 235–243.

[11] E. Kleist, T. F. Mentel, S. Andres, A. Bohne, A. Folkers, A. Kiendler-Scharr, Y. Rudich, M. Springer, R. Tillmann, J. Wildt, *Biogeosciences* **2012**, *9*, 5111–5123.

[12] A. Grira, C. Amarandei, M. N. Romanias, G. El Dib, A. Canosa, C. Arsene, I. G. Bejan, R. I. Olariu, P. Coddeville, A. Tomas, *Atmosphere* **2020**, *11*, 256.

[13] X. Wang, J. Sun, L. Bao, Q. Mei, B. Wei, Z. An, J. Xie, M. He, *J. Phys. Chem. A* **2019**, *123*, 2745–2755.

[14] L. Nondek, D. Rodler, J. W. Birks, *Environ. Sci. Technol.* **1992**, *26*, 1174–1178.

[15] J. Ehrlich, T. M. Cahill, *Atmos. Environ.* **2018**, *191*, 414–419.

[16] C. Warneke, S. L. Luxembourg, J. A. de Gouw, H. J. I. Rinne, A. B. Guenther, R. Fall, *J. Geophys. Res. Atmospheres* **2002**, *107*, ACH 6-1-ACH 6-10.

[17] T. Gao, J. M. Andino, C. C. Rivera, M. F. Márquez, *Int. J. Chem. Kinet.* **2009**, *41*, 483–489.

[18] E. Jimenez, B. Lanza, E. Martinez, J. Albaladejo, *Atmospheric Chem. Phys.* **2007**, *7*, 1565–1574.

[19] M. E. Davis, M. K. Gilles, A. R. Ravishankara, J. B. Burkholder, *Phys. Chem. Chem. Phys.* **2007**, *9*, 2240–2248.

[20] R. Atkinson, J. Arey, S. M. Aschmann, S. B. Corchnoy, Y. Shu, *Int. J. Chem. Kinet.* **1995**, *27*, 941–955.

[21] D. Rodriguez, A. Rodriguez, A. Notario, A. Aranda, Y. Diaz-de-Mera, E. Martinez, *Atmospheric Chem. Phys.* **2005**, *5*, 3433–3440.

[22] C. Kalalian, E. Roth, A. Chakir, *Int. J. Chem. Kinet.* **2017**, *50*, 47–56.

[23] E. Grosjean, D. Grosjean, J. H. Seinfeld, *Int. J. Chem. Kinet.* **1996**, *28*, 373–382.

[24] C. Kalalian, B. Samir, E. Roth, A. Chakir, *Chem. Phys. Lett.* **2019**, *718*, 22–26.

[25] M. P. O'Connor, J. C. Wenger, A. Mellouki, K. Wirtz, A. Muñoz, *Phys. Chem. Chem. Phys.* **2006**, *8*, 5236–5246.

[26] M. Duncianu, R. I. Olariu, N. Visez, V. Riffault, A. Tomas, P. Coddeville, *J. Phys. Chem. A* **2012**, *116*, 6169–6179.

[27] E. Turpin, A. Tomas, C. Fittschen, P. Devolder, J.-C. Galloo, *Environ. Sci. Technol.* **2006**, *40*, 5956–5961.

[28] R. L. Caravan, M. A. H. Khan, J. Zádor, L. Sheps, I. O. Antonov, B. Rotavera, K. Ramasesha, K. Au, M.-W. Chen, D. Rösch, *Nat. Commun.* **2018**, *9*, 1–9.

[29] I. Barnes, K. H. Becker, T. Zhu, *J. Atmospheric Chem.* **1993**, *17*, 353–373.

[30] L. Messaadia, G. El Dib, M. Lendar, M. Cazaunau, E. Roth, A. Ferhati, A. Mellouki, A. Chakir, *Atmos. Environ.* **2013**, *77*, 951–958.

[31] T. Etzkorn, B. Klotz, S. Sorensen, I. V. Patroescu, I. Barnes, K. H. Becker, U. Platt, *Atmos. Environ.* **1999**, *33*, 525–540.

[32] M. Griggs, *J. Chem. Phys.* **1968**, *49*, 857–859.

[33] R. Volkamer, P. Spietz, J. Burrows, U. Platt, *J. Photochem. Photobiol. Chem.* **2005**, *172*, 35–46.

[34] F. Reisen, S. M. Aschmann, R. Atkinson, J. Arey, *Environ. Sci. Technol.* **2003**, *37*, 4664–4671.

[35] P. Ye, X. Ding, J. Hakala, V. Hofbauer, E. S. Robinson, N. M. Donahue, *Aerosol Sci. Technol.* **2016**, *50*, 822–834.

[36] I. Al Mulla, L. Viera, R. Morris, H. Sidebottom, J. Treacy, A. Mellouki, *ChemPhysChem* **2010**, *11*, 4069–4078.

[37] E. Grosjean, D. Grosjean, *Int. J. Chem. Kinet.* **1998**, *30*, 21–29.

[38] K. Sato, B. Klotz, T. Taketsugu, T. Takayanagi, *Phys. Chem. Chem. Phys.* **2004**, *6*, 3969–3976.

[39] E. G. Colman, M. B. Blanco, I. Barnes, M. A. Teruel, *R. Soc. Chem. Adv.* **2015**, *5*, 30500–30506.

[40] M. R. McGillen, A. T. Archibald, T. Carey, K. E. Leather, D. E. Shallcross, J. C. Wenger, C. J. Percival, *Phys. Chem. Chem. Phys. PCCP* **2011**, *13*, 2842–2849.

[41] E. V. Avzianova, P. A. Ariya, *Int. J. Chem. Kinet.* **2002**, *34*, 678–684.

[42] R. Wegener, T. Brauers, R. Koppmann, S. R. Bares, F. Rohrer, R. Tillmann, A. Wahner, A. Hansel, A. Wisthaler, *J. Geophys. Res. Atmospheres* **2007**, *112*, DOI 10.1029/2006JD007531.

[43] B. Klotz, I. Barnes, T. Imamura, *Phys. Chem. Chem. Phys.* **2004**, *6*, 1725–1734.

[44] E. Gaona Colman, M. B. Blanco, I. Barnes, P. Wiesen, M. A. Teruel, *J. Phys. Chem. A* **2017**, *121*, 5147–5155.

[45] E. C. Tuazon, S. M. Aschmann, J. Arey, R. Atkinson, *Environ. Sci. Technol.* **1997**, *31*, 3004–3009.

[46] E. Grosjean, E. L. Williams II, D. Grosjean, *Sci. Total Environ.* **1994**, *153*, 195–202.

[47] E. Grosjean, D. Grosjean, *J. Atmospheric Chem.* **1997**, *27*, 271–289.

[48] R. Uchida, K. Sato, T. Imamura, *Chem. Lett.* **2015**, *44*, 457–458.

[49] H. Shen, Z. Chen, H. Li, X. Qian, X. Qin, W. Shi, *Environ. Sci. Technol.* **2018**, *52*, 10997–11006.

[50] C. Knote, A. Hodzic, J. L. Jimenez, R. Volkamer, J. J. Orlando, S. Baidar, J. Brioude, J. Fast, D. R. Gentner, A. H. Goldstein, P. L. Hayes, W. B. Knighton, H. Oetjen, A. Setyan, H. Stark, R. Thalman, G. Tyndall, R. Washenfelder, E. Waxman, Q. Zhang, *Atmospheric Chem. Phys.* **2014**, *14*, 6213–6239.

[51] A. L. Corrigan, S. W. Hanley, D. O. De Haan, *Environ. Sci. Technol.* **2008**, *42*, 4428–4433.

[52] J. Liggio, S.-M. Li, R. McLaren, *J. Geophys. Res.* **2005**, *110*.

[53] A. Lee, A. H. Goldstein, M. D. Keywood, S. Gao, V. Varutbangkul, R. Bahreini, N. L. Ng, R. C. Flagan, J. H. Seinfeld, *J. Geophys. Res.* **2006**, *111*, D07302.

[54] E. Grosjean, J. Bittencourt de Andrade, D. Grosjean, *Environ. Sci. Technol.* **1996**, *30*, 975–983.

[55] O. Horie, G. K. Moortgat, *Acc. Chem. Res.* **1998**, *31*, 387–396.

[56] J. R. Odum, T. Hoffmann, F. Bowman, D. Collins, R. C. Flagan, J. H. Seinfeld, *Environ. Sci. Technol.* **1996**, *30*, 2580–2585.

[57] R.-J. Huang, Y. Zhang, C. Bozzetti, K.-F. Ho, J.-J. Cao, Y. Han, K. R. Daellenbach, J. G. Slowik, S. M. Platt, F. Canonaco, *Nature* **2014**, *514*, 218–222.

[58] M. Corso, "Impact à court terme des particules en suspension (PM10) sur la mortalité dans 17 villes françaises, 2007-2010," can be found under /determinants-de-sante/pollution-et-sante/air/impact-a-court-terme-des-particules-en-suspension-pm10-sur-la-mortalite-dans-17-villes-francaises-2007-2010, **2015**.

[59] L. Morawska, C. He, G. Johnson, H. Guo, E. Uhde, G. Ayoko, *Environ. Sci. Technol.* **2009**, *43*, 9103–9109.

[60] C. J. Young, S. Zhou, J. A. Siegel, T. F. Kahan, *Environ. Sci. Process. Impacts* **2019**, *21*, 1229–1239.

[61] T. Liu, Z. Wang, D. D. Huang, X. Wang, C. K. Chan, *Environ. Sci. Technol. Lett.* **2018**, *5*, 32–37.

654

Table 1. Summary of experimental conditions and analytical techniques used in the present work. All experiments were performed at room temperature (298 K) and atmospheric pressure of air (1 atm) except for RASC where the initial pressure was about 400 Torr.

Kinetic studies[a]					
Reactor-Laboratory	**Reactor volume (L)**	**$[O_3]_0$ (ppm)**	**$[T2H]_0$ (ppm)**	**OH Scavenger**	**Analytical techniques**
LFR-IMT Lille Douai	10	0.555	6.5-25	Not used	- Ozone analyzer (Model 42M, Environnement SA) - GC-FID/MS (Agilent 6890-5973N)
ASC-IMT Lille Douai	300	0.113	≃4	Cyclohexane[b]	- Ozone analyzer (Model 42M, Environnement SA) - FTIR spectrometer (Thermo Nicolet 6700 with DTGS detector)
Product and SOA studies					
RASC-GSMA	63	< 1[d]	20-25	Cyclohexane[b]	- FTIR spectrometer (Brucker Equinox 55 with MCT detector) - SPME-GC/MS (Perkin-Elmer Clarus 500)
480 L glass Wuppertal	480	1.4-39	3.7-5.7	Dimethylether[c]	- FTIR spectrometer (Thermo Nicolet 6700 with MCT detector)
ASC-IMT Lille Douai	300	0.065-0.65	1.6-10.2	Not used	- SMPS (TSI, DMA 3080 and CPC 3788)

(a) Experiments carried out under pseudo-first order conditions, with $[T2H]_0/[O_3]_0 \geqslant 10$

(b) Concentration of cyclohexane between 390 and 890 ppm (ASC-SAGE) and 1540 ppm (RASC-GSMA). One experiment in ASC was performed without cyclohexane.

(c) Used as OH tracer with concentrations between 15 and 22 ppm.

(d) Ozone was introduced continuously into RASC at a low flow rate.

Table 2. Kinetic results for T2H + O_3 in ASC and LFR. Uncertainties correspond to 2σ.

Reactor type	**$[T2H]_0$ (ppm)**	**$[O_3]_0$ (ppm)**	**Method**	**k (× 10^{18} cm^3 $molecule^{-1}$ s^{-1})**	**Reference**
Flow reactor	6.5-25	0.555	Absolute, T2H in excess	1.52 ± 0.19	**This work**
Chamber	1	0.2	Relative	2.00 ± 1.00	[20]
Chamber	2.34-3.5	0.073-0.114	Absolute, T2H in excess	1.28 ± 0.28	[23][a]
Chamber	0.81-24	40-200	Absolute, O_3 in excess	1.37 ± 0.03	[22][a]

[a] Not specified if 1σ or 2σ.

Table 3. Product formation yields of the ozonolysis of T2H from this work and comparison with literature data.

Presence of OH scavenger	Identified products	Yield (%)	References
No scavenger	Glyoxal	48 ± 10	This work (480-L)
	Butanal	33 ± 7	
	Acetaldehyde	Not quantified	
	Propanal	Not quantified	
Scavenger (Cyclohexane)	Glyoxal	59 ± 15	This work (RASC)
	Butanal	36 ± 9	
	Acetaldehyde	10 ± 3	
	Propanal	19 ± 5	
	2-hydroxybutanal	18 ± 6 [a]	
Scavenger (Cyclohexane)	Glyoxal	52.7 ± 5.5	[23]
	Butanal	55.9 ± 3.7	
	Acetaldehyde	10.9 ± 2	
	Propanal	6.7 ± 0.8	
	2-oxobutanal or 2-hydroxybutanal [b]	7.4 ± 0.6	

a: average of IR and GC analysis

b: Grosjean et al.[23] were not able to distinguish between the two carbonyls (see text).

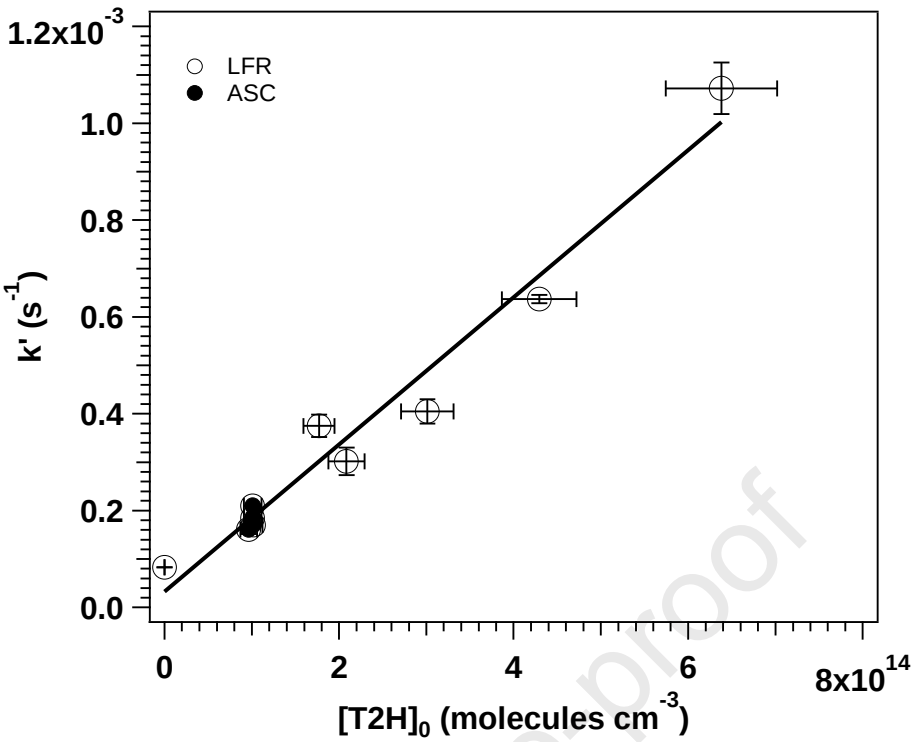

Figure 1. Plot of k' versus the initial concentration of T2H at room temperature performed in LFR (open symbols) and in ASC (filled symbols). The regression fit was carried out on both LFR and ASC data.

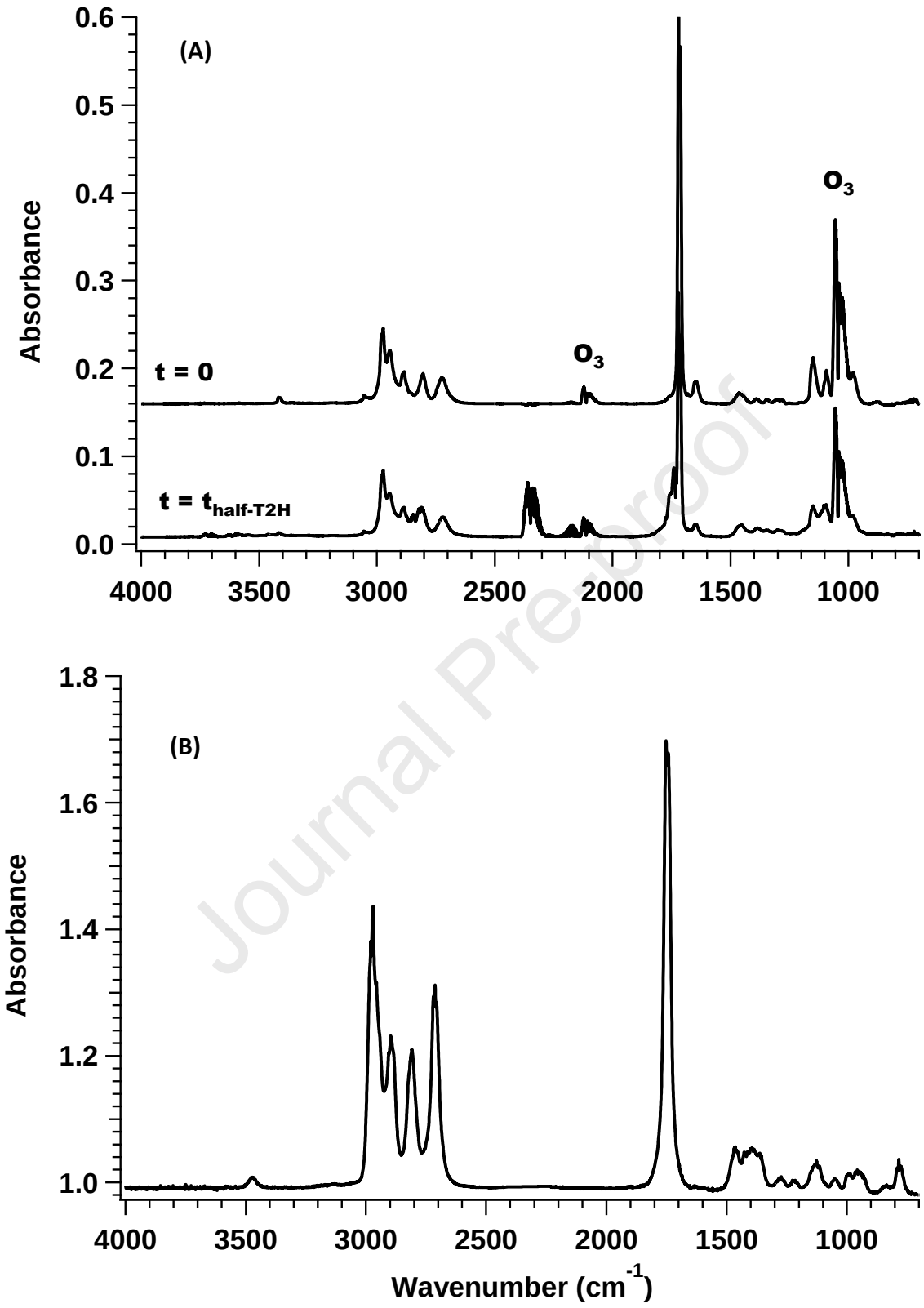

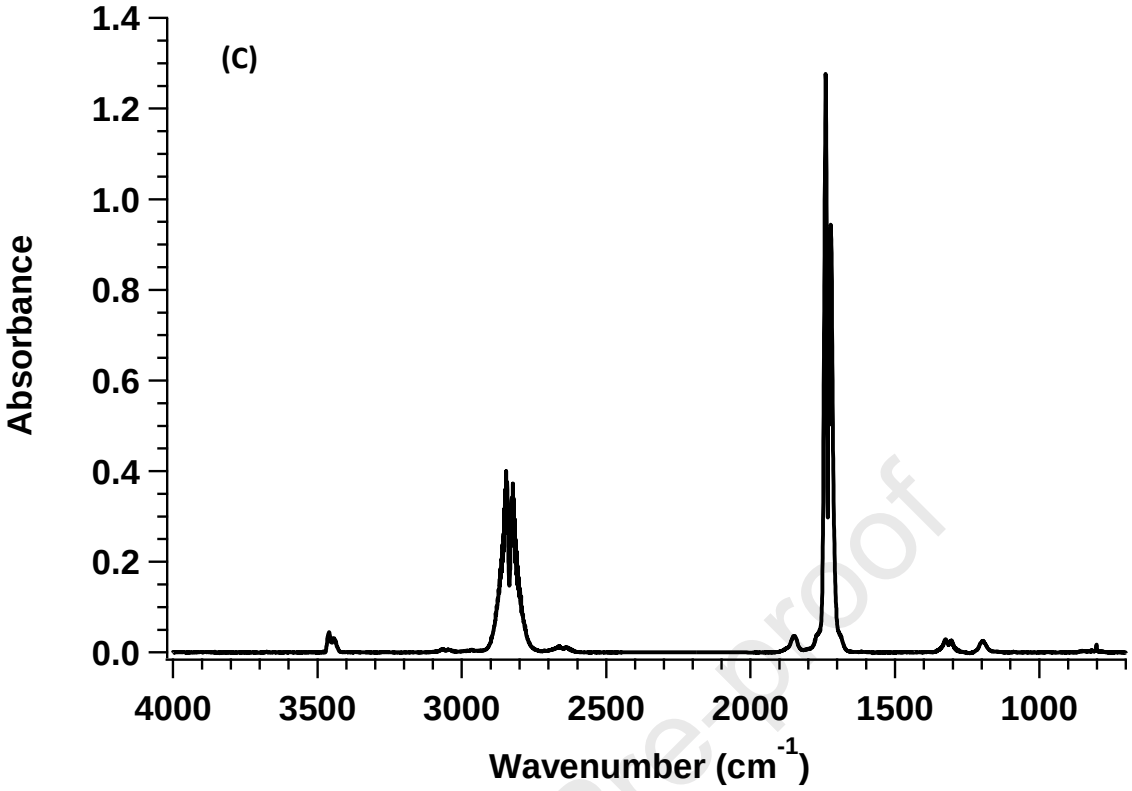

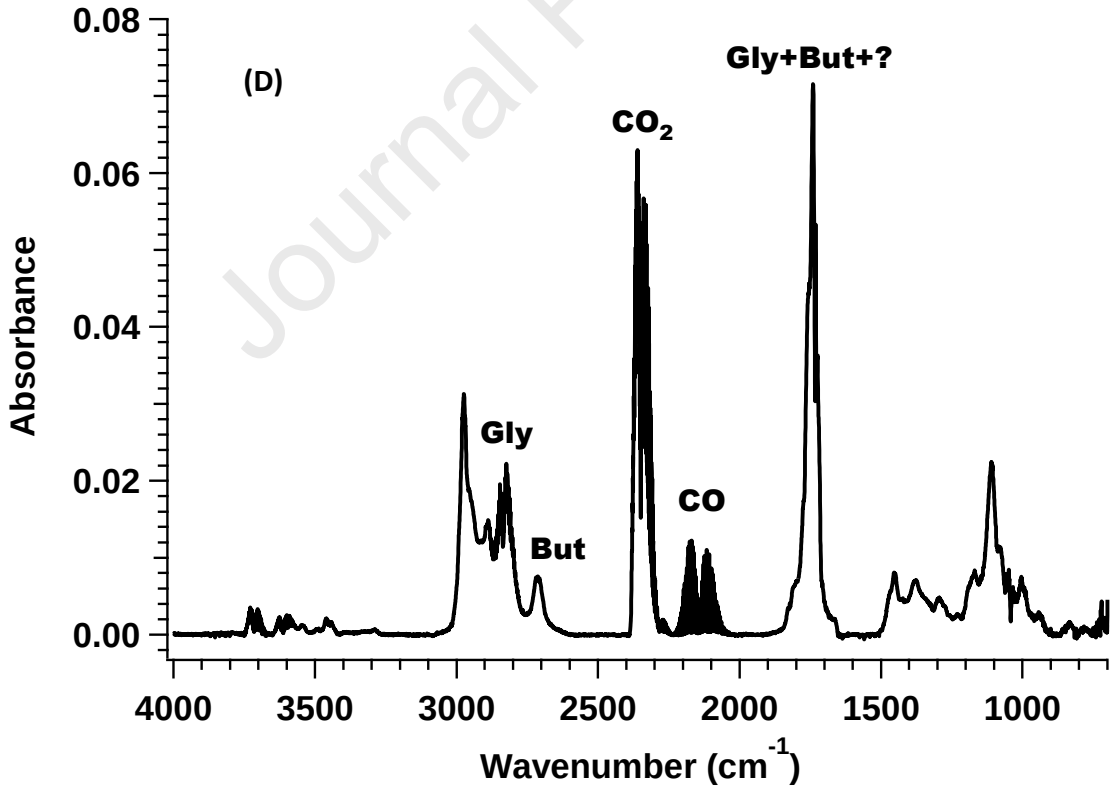

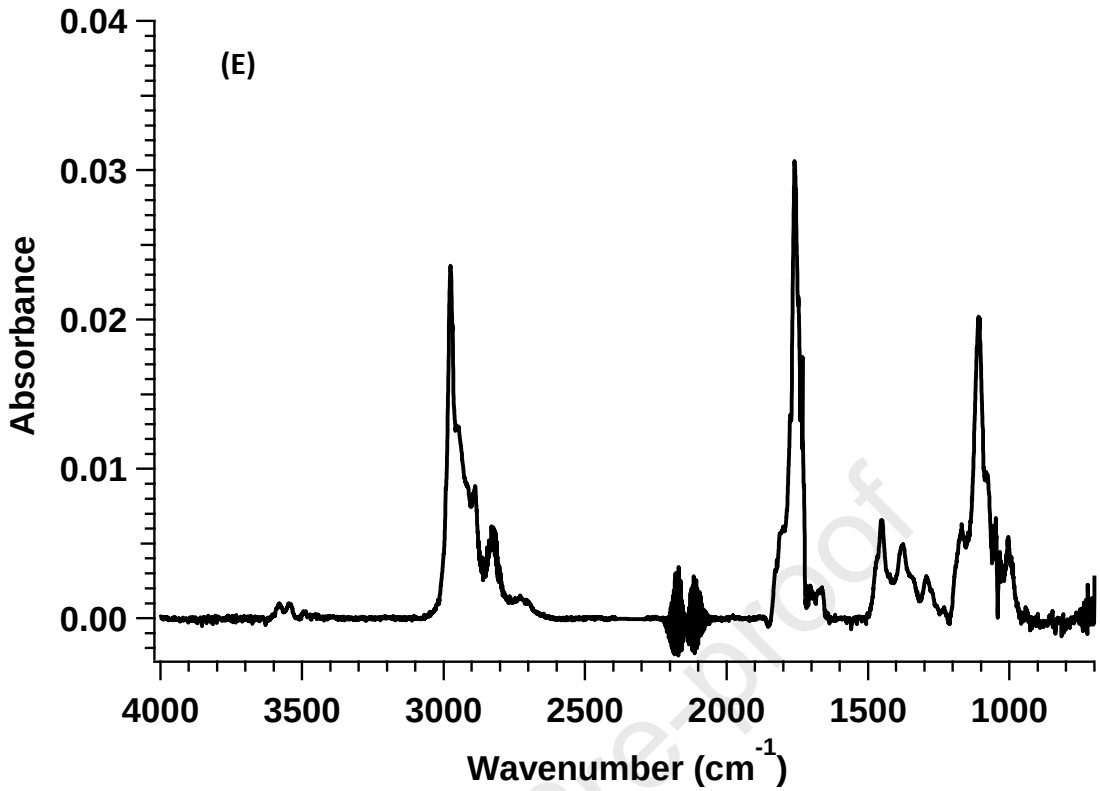

Figure 2. IR spectra obtained in the 480 L reactor. From bottom to top: Panel A shows the IR spectrum at t = 0 (O_3 bands are annotated; the other bands correspond to T2H) and after 50% T2H has reacted. Panels B and C show the reference spectra of butanal and glyoxal, respectively. Panel D displays the residual IR spectrum after removing T2H and O_3 (where Gly and But represent glyoxal and butanal, respectively). Panel E corresponds to the residual after removing butanal and glyoxal.

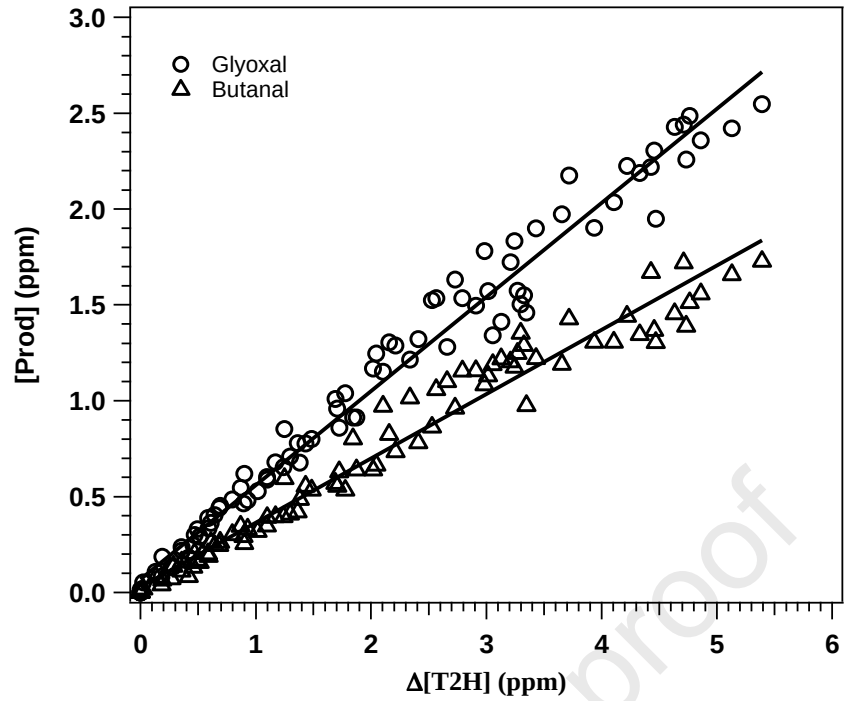

Figure 3. Plots of the concentrations of the glyoxal (○) and butanal (△) as a function of reacted T2H (FTIR analysis) obtained in the 480-L chamber (without OH scavenger)

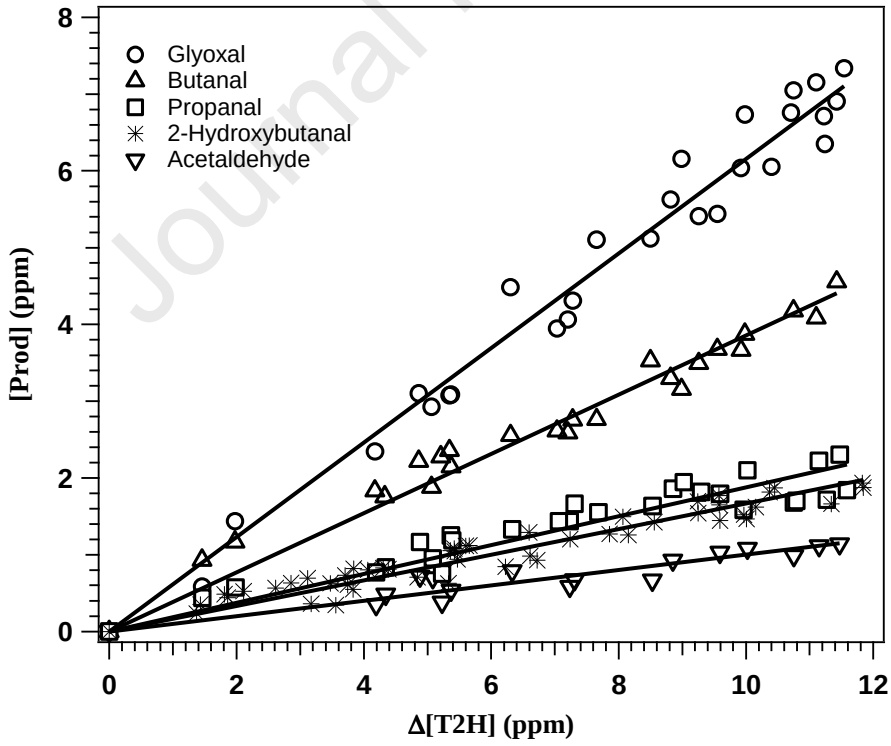

Figure 4. Plots of the concentrations of all the reaction products (GC-MS analysis) as a function of reacted T2H obtained in RASC (with OH scavenger)

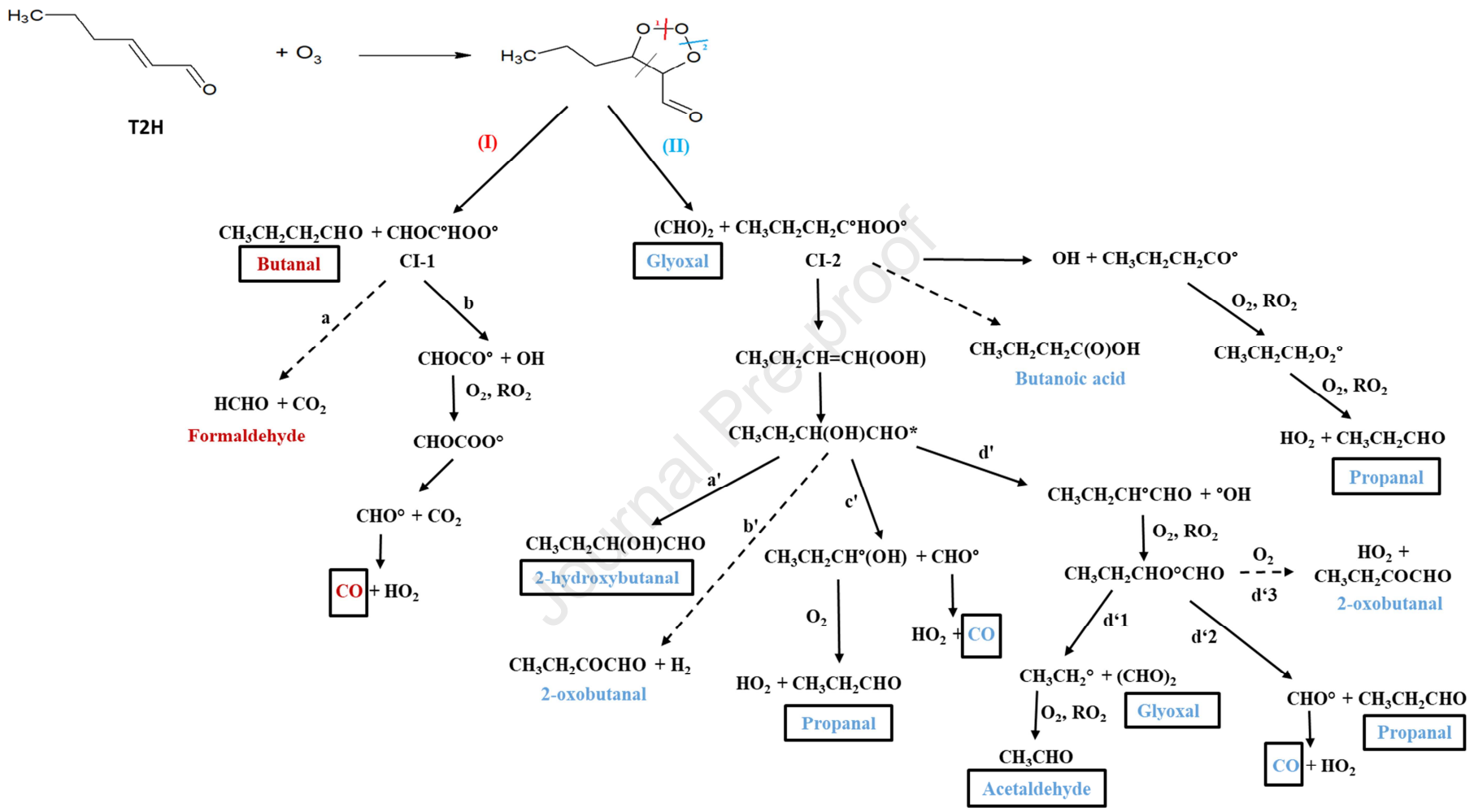

Figure 5. Proposed mechanistic scheme for the ozonolysis of T2H; framed products correspond to those identified in FTIR and GC/MS with and without an OH scavenger. Products from channel (I) are in red; products from channel (II) are in blue. Dashed arrows indicate reaction pathways that are negligible or not confirmed by the present results.

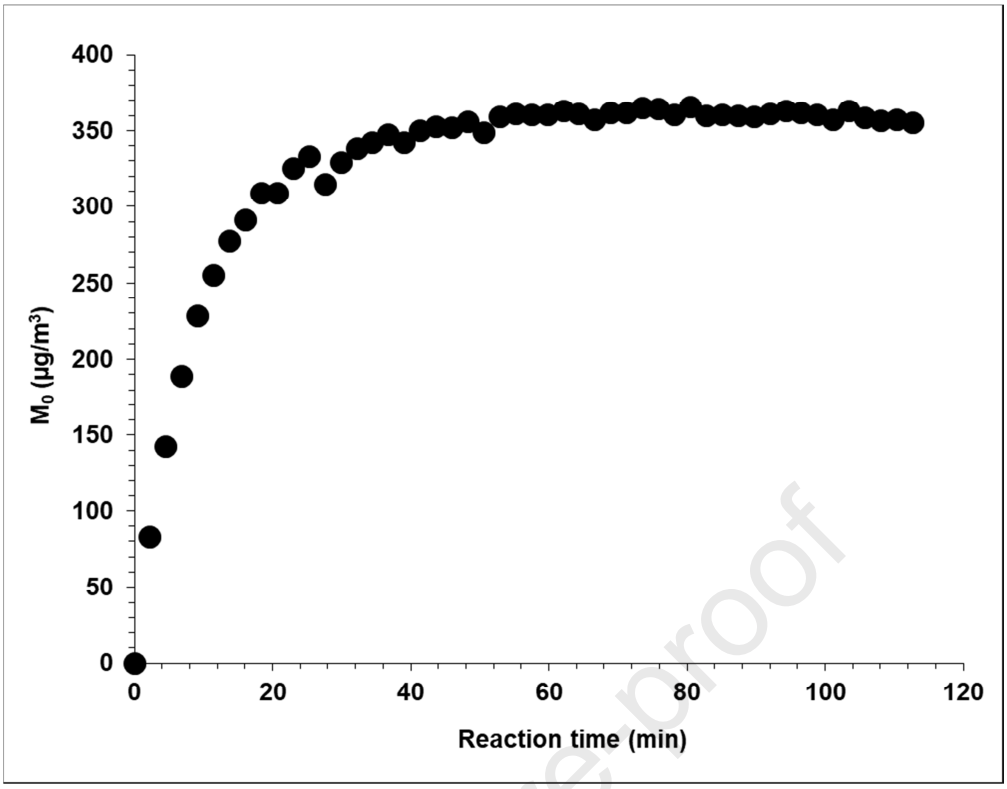

Figure 6. SOA formation as a function of time for T2H in ASC chamber (with $[T2H]_0$ = 3.8 ppm and $[O_3]_0$ = 390 ppb).

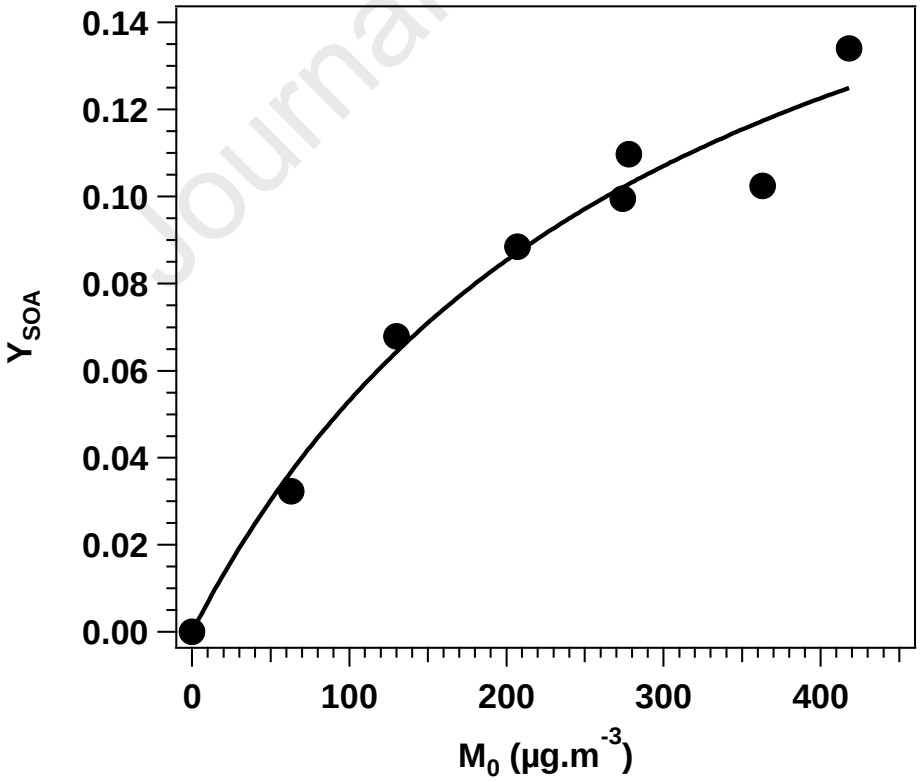

Figure 7. SOA formation yields Y_{SOA} vs. aerosol mass concentrations for T2H in ASC. The fit is carried out using Odum's one-product model (Eq. 5).

- Trans-2-hexenal ozonolysis kinetics and products investigated
- A reaction mechanism is proposed.
- First secondary organic aerosol investigation

Declaration of interests

☒ The authors declare that they have no known competing financial interests or personal relationships that could have appeared to influence the work reported in this paper.

☐The authors declare the following financial interests/personal relationships which may be considered as potential competing interests: